

Ultrasensitive Boron–Nitrogen-Codoped CVD Graphene-Derived NO₂ Gas Sensor

Shubhda Srivastava, Prabir Pal, Durgesh Kumar Sharma, Sudhir Kumar, T. D. Senguttuvan,* and Bipin Kumar Gupta*



Cite This: *ACS Mater. Au* 2022, 2, 356–366



Read Online

ACCESS |

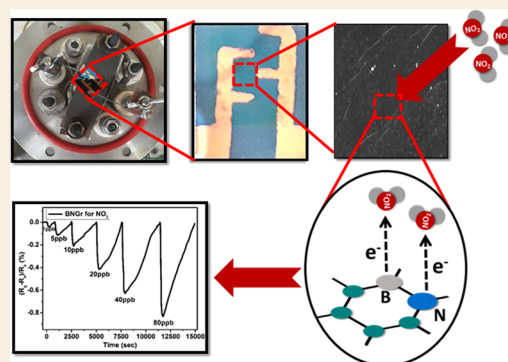
Metrics & More

Article Recommendations

Supporting Information

ABSTRACT: Recent trends in 2D materials like graphene are focused on heteroatom doping in a hexagonal honeycomb lattice to tailor the desired properties for various lightweight atomic thin-layer derived portable devices, particularly in the field of gas sensors. To design such gas sensors, it is important to either discover new materials with enhanced properties or tailor the properties of existing materials via doping. Herein, we exploit the concept of codoping of heteroatoms in graphene for more improvements in gas sensing properties and demonstrate a boron- and nitrogen-codoped bilayer graphene-derived gas sensor for enhanced nitrogen dioxide (NO₂) gas sensing applications, which may possibly be another alternative for an efficient sensing device. A well-known method of low-pressure chemical vapor deposition (LPCVD) is employed for synthesizing the boron- and nitrogen-codoped bilayer graphene (BNGr). To validate the successful synthesis of BNGr, the Raman, XPS, and FESEM characterization techniques were performed. The Raman spectroscopy results validate the synthesis of graphene nanosheets, and moreover, the FESEM and XPS characterization confirms the codoping of nitrogen and boron in the graphene matrix. The gas sensing device was fabricated on a Si/SiO₂ substrate with prepatterned gold electrodes. The proposed BNGr sensor unveils an ultrasensitive nature for NO₂ at room temperature. A plausible NO₂ gas sensing mechanism is explored via a comparative study of the experimental results through the density functional theory (DFT) calculations of the adsorbed gas molecules on doped heteroatom sites. Henceforth, the obtained results of NO₂ sensing with the BNGr gas sensor offer new prospects for designing next-generation lightweight and ultrasensitive gas sensing devices.

KEYWORDS: NO₂ sensing, CVD graphene, B- and N-codoping, gas sensor



1. INTRODUCTION

In the modern scenario, air contamination is undoubtedly one of the most irresistible problems faced by our planet.¹ The constant upswing in the release of various toxic gases from many industries and household activities has triggered a severe risk to both human health and the environment. Detection of these hazardous gases is a very essential and crucial job in some situations like explosive detection, emission, and environmental monitoring.^{2–4} Nitrogen dioxide (NO₂) is one of the most toxic air pollutants and is largely released by the burning of remnant fuel and organic plants. The concentrations of NO₂ greater than 1 ppm can be very dangerous to the respiratory system of human beings.² In addition, it takes part in acid rains and ozone (O₃) formation, which aggravate smog.² Therefore, very extensive monitoring of a very dash amount of it is required for air quality observation, health protection, and environmental control.⁵ As per EPA (Environmental Protection Agency of U.S.),⁶ only 53 ppb NO₂ could be set as an annual threshold limit.⁷ Usually, for an ideal gas sensor, the limit of detection (LOD) should always be lower than the threshold value. Thus, there is an intensive requirement to

continuously grow newer materials for better gas sensors for this toxic gas. In this context, graphene has been considered a big base for designing a lightweight, ultrathin, and portable gas sensing device for many toxic gases.^{8–13} Being a perfect two-dimensional material with an atomic thin-layer structure, graphene has received massive attention for application in gas sensing because atomically thin structures are considered ideal for gas molecules' adsorption and desorption.¹³ Additionally, the concept of introduction of defects and dopants in the graphene lattice has further enhanced the sensing properties of pure graphene.^{14–17}

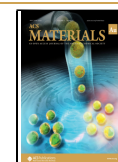
It is very interesting that boron (B), nitrogen (N), and carbon (C) can atomically be mixed to have different hexagonal structures with variable ratios.^{18–20} Several theoretic-

Received: January 6, 2022

Revised: February 3, 2022

Accepted: February 3, 2022

Published: February 21, 2022



cal and few experimental studies have shown that electronic properties can be easily tuned with BCN structures. It has the similar effect of small change in band gap of graphene as the individual doping of B and N does.^{20–26} In a recent study, graphene with BN domains has been synthesized, which shows a small band gap of ~ 18 meV.²⁷ Although there are a number of reported theoretical works on the synthesis of codoping of B and N in the graphene lattice, experimental work in this direction has been lacking. Therefore, the codoping of more than one element in graphene may generate some new properties and synergistic interactions between graphene and gas molecules for gas sensing applications. Few experimental^{28–30} as well as theoretical^{31–33} reports have shown that the codoping of two or more heteroatoms in graphene is very useful for further improvement in the surface reactivity of graphene and hence the enhancement in its sensing performance. Niu et al.³⁴ studied that the simultaneous doping of N and Si atoms in graphene can effectively alter the sensing capability for NO₂ gas. Recent reports have presented that codoping of B and N atoms in graphene is capable of providing excellent electronic properties with the combined effect of B and N.³⁵ Codoping of B and N has higher catalytic activity than individual doping of B and N.^{36,37}

Here, we present an organized experimental as well as theoretical study to explore B- and N-codoped graphene nanosheets for NO₂ gas sensing applications. In the literature, there are few articles on the theoretical study of the gas sensing behavior of B- and N-codoped graphene nanosheets but no experimental report is reported so far. With the findings of this work, we present here an experimental report on CVD-grown BNGr nanosheets for NO₂ gas sensors. The trace-level concentrations (i.e., ppb level) of NO₂ have been studied at room temperature. BNGr nanosheets have been prepared using the low-pressure chemical vapor deposition (LPCVD) method. Methane was used as a C source and borazane (H₃NBH₃) as a B and N source for the synthesis of undoped graphene (Gr) and BNGr nanosheets. The significant changes in the gas sensing properties of the BNGr gas sensor for different low concentrations of NO₂ gas are studied along with the comprehensive DFT study to explore and identify the interaction between gas molecules and BNGr nanosheets. We also discuss in detail the sensing mechanism of NO₂ gas by the BNGr gas sensor. The outcomes of this work may be beneficial toward designing an efficient CVD graphene-based ultrathin gas sensor for trace-level detection of NO₂ pollutants.

2. EXPERIMENTAL SECTION

2.1. Synthesis of Boron (B)- and Nitrogen (N)-Codoped Graphene Nanosheets

A copper (Cu) foil with a thickness of 0.025 μm and 99.99% purity (Alfa Aesar) was used for the growth of pure Gr and BNGr nanosheets using methane (CH₄) as a C precursor and borazane (H₃NBH₃) as the sole source of B and N. First, a 2×3 cm² piece of Cu foil was placed in the center of the heating zone of the quartz tube furnace having a horizontal length of 2.5". The tube was then evacuated to a base pressure of 0.01 Torr, and then a total pressure of ~ 11.9 Torr was maintained inside the tube by flowing hydrogen (H₂) and argon (Ar) gases continuously. Under these flow conditions, heating was started at 10 °C/min to reach 950 °C. As soon as the temperature reached 950 °C, annealing started. In the meantime, heating of borazane at 100 °C was performed in a separate quartz tube connected with the main tube to obtain the BN content. After annealing for 30 min, methane and borazane vapors were led into the quartz tube for graphene growth. At the time of growth, the total

pressure inside the tube was kept at ~ 31.9 Torr. After the growth for 3 min, the flow of methane and borazane was closed and the BNGr nanosheet on Cu was allowed to cool quickly with the continuous flow of Ar and H₂. Here, we used a sole precursor, i.e., borazane (H₃NBH₃), for the doping B and N both. By controlling the heating temperature and time of heating, the amount of B and N can be controlled. The Gr nanosheet sample was synthesized in the same LPCVD setup using methane as a C source for comparative studies in gas sensing. While the synthesis of Gr, the total pressure inside the tube was ~ 48 Torr, with the partial pressure of H₂. To avoid airborne contaminations, all of the grown graphene samples were kept in vacuum desiccators for further use. The LPCVD setup used for the BNGr nanosheet synthesis is presented in Figure S1.

2.2. Gas Sensor Device Fabrication

Further, to fabricate the gas sensing device, the grown nanosheets were then transferred on Si/SiO₂ substrates with prepatterned gold (Au) electrodes. The prepatterns of Au having a width of 1 mm, an interdigit spacing of 1.5 mm, and an electrode area of 10×10 mm² were deposited using a thermal evaporation system. In the process of transfer, a thin layer of PMMA was coated on the top layer of graphene films using a spin coater and air-dried. Afterward, to etch Cu, this assembly of PMMA/graphene/Cu foil was put in a 3:1 solution of water and nitric acid and set aside overnight for total etching of Cu. Now, the graphene film with the PMMA layer was taken out on the desired Si/SiO₂ substrate with Au electrodes. For characterization, the graphene films on PMMA were taken on Si/SiO₂ substrates, a quartz substrate, and TEM grids. Further, cleaning was performed by repeatedly dipping the substrate in DI water and IPA and then drying it under nitrogen (N₂) gas. In the end, the PMMA/graphene assembly on Si/SiO₂ was dipped in acetone for a few minutes to dissolve the thin layer of PMMA. This transferred graphene was further used as a gas sensor device for the gas sensing property study and *I*–*V* characteristic measurements while the other transferred graphene nanosheets on the Si/SiO₂ substrate, quartz substrate, and TEM grids for further characterization.

2.3. Material Characterization

The synthesized samples were then validated by Raman spectroscopy (InVia Raman Microscope, Renishaw), field emission scanning electron microscopy (FESEM), energy-dispersive X-ray spectroscopy (EDX), X-ray photoelectron spectroscopy (XPS), and a UV-1800 Shimadzu spectrophotometer. For Raman measurements, an excitation laser with a wavelength of 514.5 nm was used. The XPS measurements were performed using a scanning X-ray microprobe system equipped with a monochromatic aluminum K α high flux focused X-ray source with a photon energy of 1486.7 eV and a multichanneltron hemispherical electron energy analyzer (PHI 5000 VERSAPROBE II, Physical Electronics system). The binding energy was calibrated by measuring C 1s at 284.6 eV. The total energy resolution, estimated from the width of the Fermi edge, was about 400 meV for a monochromatic aluminum K α line with a pass energy of 11.750 eV. A charge neutralizer was used to compensate the surface charging of the samples.

2.4. Gas Sensing Characterization

The indigenously developed sensing setup with a stainless steel chamber was used for performing the gas sensing measurements. An Agilent B2901A precision source meter was used to record the change in resistance by applying a constant voltage of 0.5 V. With the controlled procedure of gas injection, the concentrations of NO₂ were varied. Before every repeated cycle of testing, the chamber was evacuated to its base pressure of 10⁻¹ Torr using a rotary pump. For calculating the response of the sensors, the following relation was used

$$S(\%) = \left[\frac{(R_g - R_a)}{R_a} \right] \times 100$$

Here, R_a and R_g denote the resistances of the sensor in air and gas, respectively.

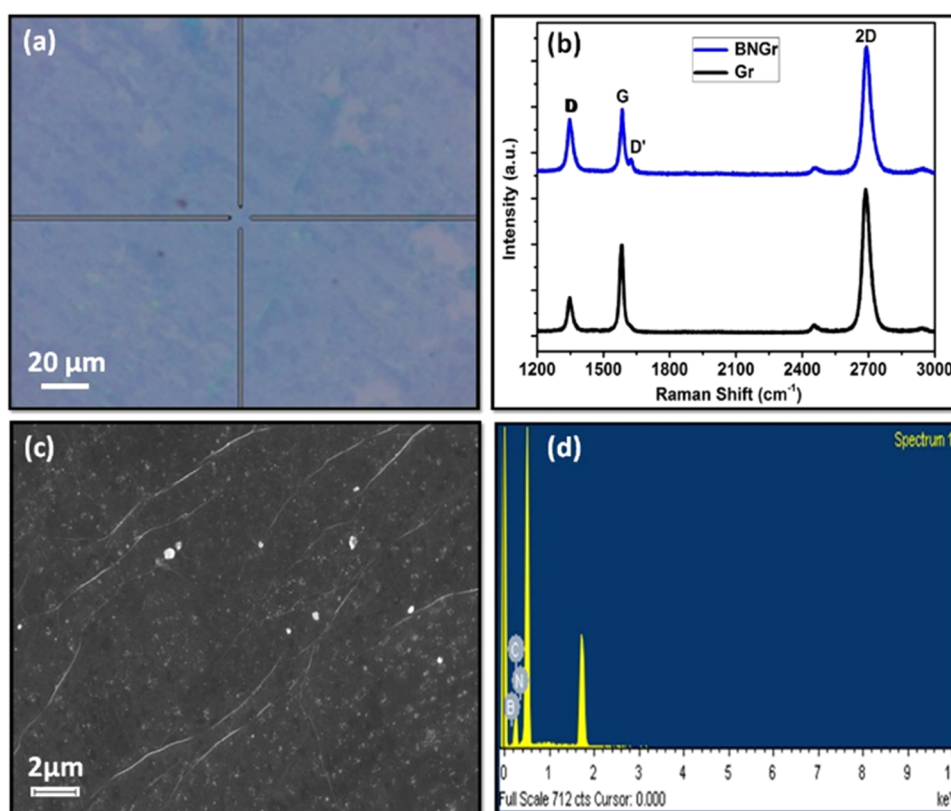


Figure 1. (a) Optical microscopy image of the BNGr nanosheet. (b) Raman spectra of Gr and BNGr nanosheets. (c) FESEM image of the BNGr nanosheet. (d) EDX spectrum of the small region of the BNGr nanosheet with elements B, N, and C present in the nanosheet.

2.5. Computational Methods

First-principles density functional theory (DFT) calculations were performed using the Vienna Ab initio Simulation Package (VASP),³⁸ which incorporates the projected augmented wave (PAW) method for the atomic potential, which includes core electron effects on valence electrons. The Perdew–Burke–Ernzerhof (PBE)³⁹ form of the generalized gradient approximation (GGA) exchange–correlation functional was considered in all sets of computations. We included the van der Waals (vdW) interaction between adsorbed NO₂ gas molecules and graphene sheets and used Grimme’s suggested DFT-D3⁴⁰ functional in the structure optimization, which provided good agreement for the distance between adsorbed NO₂ gas molecules and graphene nanosheets. For the expansion of plane wave basis sets, the kinetic energy cutoff equal to 550 eV was supplied. The Gaussian smearing method was used for integrating the first Brillouin zone (BZ) with a mesh of *k*-points of size 6 × 6 × 1 centered at Γ . An energy convergence criterion of 10^{−6} eV was considered in all sets of calculations. Atomic relaxation using the conjugate gradient approximation was followed to reduce the magnitude of the Hellmann–Feynman force up to ≤0.01 eV/Å. The unit cell of graphene was modeled hexagonally to calculate the adsorption of NO₂ gas molecules over it. The graphene unit cell was extended by multiplying 5 × 5 × 1, which resulted in a supercell with a total of 50 atoms of C. The stability of the system was predicted in terms of adsorption energy (E_{ads}) calculations by the following equation

$$E_{\text{ads}} = E_{(\text{graphene}+\text{gas})} - E_{\text{graphene}} - E_{\text{gas}}$$

where $E_{(\text{graphene}+\text{gas})}$ and E_{graphene} denote the total energies of NO₂ gas molecules adsorbed on Gr or BNGr nanosheets and the total energy of Gr or BNGr, respectively. The term E_{gas} is the total energy of isolated NO₂ gas molecules considered in a cubic box.

Further, to understand the interaction between Gr or BNGr nanosheets and adsorbed NO₂ gas molecules, we calculated the electronic charge difference by the following formula

$$\rho = \rho_{(\text{graphene}+\text{gas})} - \rho_{\text{graphene}} - \rho_{\text{gas}}$$

where $\rho_{(\text{graphene}+\text{gas})}$ and ρ_{graphene} represent the total charge of NO₂ gas molecule adsorbed on Gr or BNGr nanosheets and total charge on Gr or BNGr nanosheets respectively while ρ_{gas} is the total charge on NO₂ gas molecule only.

3. RESULTS AND DISCUSSION

First, the optical images of the BNGr nanosheet on the Si/SiO₂ substrate were recorded, as shown in Figure 1a. Raman spectroscopy is the best-suited system for graphene nanosheet confirmation. The Raman spectra of Gr and BNGr nanosheets were recorded, as depicted in Figure 1b. The Raman spectrum of the Gr nanosheet shows three dominant peaks, which represent a D band at 1347 cm^{−1}, a G band at 1583 cm^{−1}, and a 2D band at 2686 cm^{−1} (Table 1).³² In the spectrum, the D

Table 1. Peak Positions and Ratios of Intensities of the Raman Spectra of Gr and BNGr Nanosheets

sample	D peak (cm ^{−1})	G peak (cm ^{−1})	D' peak (cm ^{−1})	2D peak (cm ^{−1})	I_{2D}/I_G	I_D/I_G	$I_D/I_{D'}$
Gr	1347	1583		2686	1.63	0.40	
BNGr	1347	1585	1624	2691	1.94	0.85	3.50

band intensity is too low compared with G and 2D bands, which signifies the good quality of graphene nanosheets.⁴¹ Further, the ratio of intensities of 2D and G bands is around 1.63, which indicates the bilayer nature of the graphene nanosheet. The Raman spectrum of BNGr also exhibited three dominant peaks representing the three bands i.e., D band at 1347 cm^{−1}, G band at 1585 cm^{−1}, and 2D band at 2691 cm^{−1}, as given in Table 1. The small upshift in G and 2D bands for

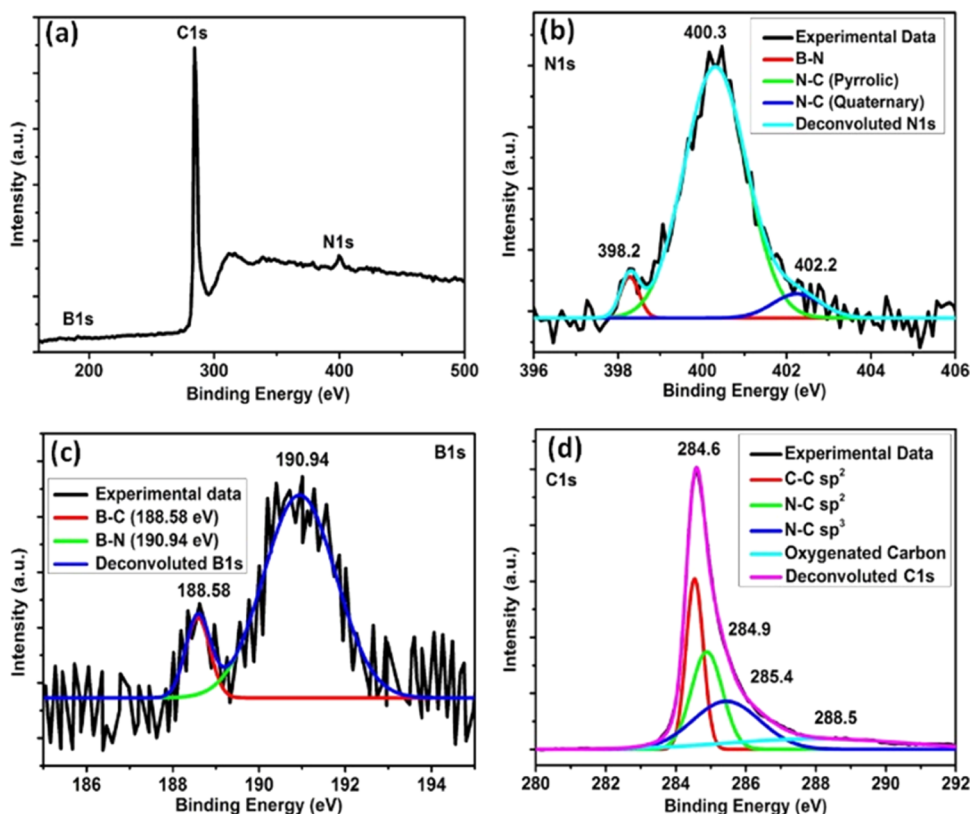


Figure 2. (a) Survey scan spectra of the BNGr nanosheet. Deconvoluted (b) N 1s core-level spectra, (c) B 1s core-level spectra, and (d) C 1s core-level spectra of the BNGr nanosheet on the Si/SiO₂ substrate.

BNGr is because of the doping in the graphene lattice.⁴² The doping in BNGr can further be validated by the presence of the D' peak as a shoulder of the G peak at 1624 cm⁻¹. This splitting of the G peak in G and D' peaks in B- and N-codoped graphene²⁷ has already been reported in several studies, which indicates the break in the local symmetry of graphene due to heteroatom doping.^{43–45} The intensity ratio of 2D and G bands was calculated and found to be 1.94, which again shows the bilayer nature of the BNGr nanosheet. The higher intensity of the D band in the BNGr nanosheet compared to the Gr nanosheet could be due to the defects introduced in the form of doping in the graphene lattice. The intensity ratio of D and D' shows the nature of defects in graphene. Further, an increase in the I_D/I_G ratio, as shown in Table 1, indicates the incorporation of dopants in graphene.

Figure 1c,d (Figure S2a,b) depicts the FESEM images and EDX spectrum of the BNGr (Gr) nanosheet on the Si/SiO₂ substrate. In Figure 1c, the sheet-like arrangement with some wrinkles on it clearly shows the synthesis of graphene nanosheets. The EDX spectrum of BNGr nanosheets in Figure 1d shows the presence of all elements in it. The EDX spectrum of BNGr clearly displays the presence of C, B, and N elements in the graphene sample. The EDX spectra of the small area of the Gr nanosheet in Figure S2b clearly show the presence of the C element only. The two images (optical and FESEM) have been recorded at two different selective places with different magnifications. The small white-colored dots in the SEM image could be some foreign particles from ambient during SEM imaging. The lined structures in the SEM image are the wrinkles of the graphene sheet.

The XPS data of Gr and BNGr samples were recorded for clear validation of chemical bondings in nanosheets on the Si/

SiO₂ substrate. Figures 2 and S3 show the XPS spectra of BNGr and Gr nanosheets, respectively. The XPS data of Gr (Figure S3) show the presence of one peak for C atoms only, while the XPS survey scan spectra of BNGr in Figure 2a by contrast shows three main peaks at 284, 191, and 400 eV, which correspond to C, B, and N atoms, respectively. Table 2 shows the atomic percentages of C, B, and N as 86.84, 2.76, and 1.87%, respectively. The BNGr sample also contains 8.56% of oxygen (O).

Table 2. Atomic Percentage of Elements Present in the BNGr Nanosheet

sample	carbon (C) (at %)	boron (B) (at %)	nitrogen (N) (at %)	oxygen (O) (at %)
BNGr	86.84	2.76	1.84	8.56

Figure 2b shows the N 1s core-level spectra of the BNGr nanosheet. The further deconvolution of this N 1s peak gives three subpeaks, out of which the main peak at 398.2 eV can be accredited to B–N bonds.⁴⁶ As per reports, pure boron nitride nanosheets (h-BN)⁴⁷ and BN-doped graphene²⁷ nanosheets with distinct BN domains show a peak at 398.1 eV. Another two peaks at 400.3 and 402.2 eV may be because of the existence of N–C bonds.^{48,49} The highest peak at 400.3 eV confirms the pyrrolic N-type bonding. Pyrrolic N indicates the presence of N atoms in the π conjugated system and donates two p-electrons to the π system.⁵⁰ Another peak at 402.2 eV denotes the graphitic or quaternary N type of atom, which means that the N atoms replace C atoms within the graphene lattice. The N 1s peak is more intense toward the higher binding energies of N–C bonds. This advises that more N–C

bonds are present compared to B–N bonds. Table 3 displays the contributions of the B–N- and N–C-type bonds in BNGr.

Table 3. Percentage of B–N and N–C Bonds in the BNGr Nanosheet

sample	B–N		N–C (pyrrolic)		N–C (quaternary)	
	BE (eV)	ratio (%)	BE (eV)	ratio (%)	BE (eV)	ratio (%)
BNGr	398.2	13.57	400.3	80.25	402.2	6.18

Figure 2c shows the B 1s core-level spectra of the BNGr nanosheet, which suggests that two types of species at 190.94 and 188.58 eV with different intensities are present in the doped graphene nanosheets. The higher peak at 190.94 may be related to the B–N bonding structure^{51–53} and competes well with the B peak present in the h-BN structure.⁵⁴ The presence of peaks at 398.2 eV in N 1s spectra and at 190.94 eV in B 1s spectra of BNGr together proves the presence of B–N bonds in the sample and correlates the result with the reported data for h-BN structure films.⁵⁴ Another peak with a lower concentration at 188.58 eV may correspond to BC₃, which further suggests that B–C-type bonds are also there in the doped BNGr nanosheets.^{55,56} However, the B–C bonds with lower intensity confirm that B–N formation in BNGr nanosheets are more favorable than B–C bonds. Figures 2d and S3 show the C 1s core-level spectra of BNGr and Gr nanosheets. After deconvolution, the C 1s core-level spectra of BNGr nanosheets show four peaks. The main peak at 284.6 eV can be allotted to graphitic-type sp² C (C–C bond) in BNGr, which arises from the undoped areas of graphene.⁵⁷ Another two peaks at 284.9 and 285.4 eV match up with sp² C atoms and sp³ C atoms bonded to N atoms (N–C bond), respectively.^{46,58} The next smaller peak at 288.5 eV may be accredited to oxygenated C atoms.⁵⁹ Further, the deconvolution of C 1s core-level spectra of the Gr nanosheet gives four subpeaks, out of which the main peak at 284.6 eV denotes the C–C bond, and the other smaller peaks at 284.9, 285.5, and 287.5 eV show the C–OH, C–O, and O–C=O bonds, respectively.^{60,61} A combined O 1s core-level spectra of Gr and BNGr have also been plotted and shown in Figure S4 to investigate the oxygen content in the doped and undoped graphene nanosheets. It has been found from Figure S4 that the oxygen content decreases from pure to B- and N-codoped graphene nanosheets.

The absorption studies have also been performed further to realize the optical characteristics of the BNGr nanosheet. Figure 3a shows the UV–vis spectra of Gr and BNGr nanosheets taken on quartz substrates. A wide absorption peak can be seen at 268 nm in the case of Gr, which refers to the resonant excitonic effect. This effect generates because of the interaction of electrons and holes in π and π^* bands at point M.^{62,63} It is clear from Figure 3a that as soon as B and N are inserted in the pure graphene lattice, the π -plasmon peak intensity decreases and a broad peak at 200 nm appears. This peak at 200 nm resembles the absorption peak of h-BN.²⁷ The presence of the peak at 200 nm because of BN bonding supports the results of XPS analysis, and the presence of the peak at 268 nm clears the presence of the undoped regions of graphene.

I–*V* measurements of both the nanosheets were performed on a Si/SiO₂ substrate with the applied voltage from –0.1 to 0.1 V before exposing the nanosheet sensors to NO₂ gas, as shown in Figure 3b. The *I*–*V* curves with linear behavior indicate the good ohmic contact of the deposited Gr and BNGr nanosheets with gold contacts. Also, as shown in Figure 3b, the decrease in the current value of BNGr compared to Gr is obvious because of B and N doping.

The gas sensing properties of Gr- and BNGr-based sensors were tested in an indigenously developed sensing setup (Figure S5) by exposing the sensors to NO₂ gas and recording the corresponding resistance change with time. The static flow of NO₂ was applied at ambient conditions for all measurements. Before every measurement, the test chamber was flushed with a rotary pump, then the test gas was injected, and the corresponding resistance change with time was noted. Again, the p-type nature of both the sensors was confirmed by observing the decrease in resistance upon exposure to an oxidizing gas, i.e., NO₂. For recovery, the sensors were flushed with a rotary pump and exposed to ambient conditions.

Room-temperature measurements were performed for all of the sensors. The sensing characteristics of both the sensors were evaluated by monitoring the alterations in their resistances with time when exposed to the different concentrations of gas. Figure 4 shows the responses of the BNGr sensor for different concentrations of NO₂ gas. It is clearly visible from Figure 4a that the resistance decreases immediately when NO₂ is injected, which may be due to charge transfer between BNGr and adsorbed NO₂ gas molecules. Notably, the sensor response of the BNGr sensor

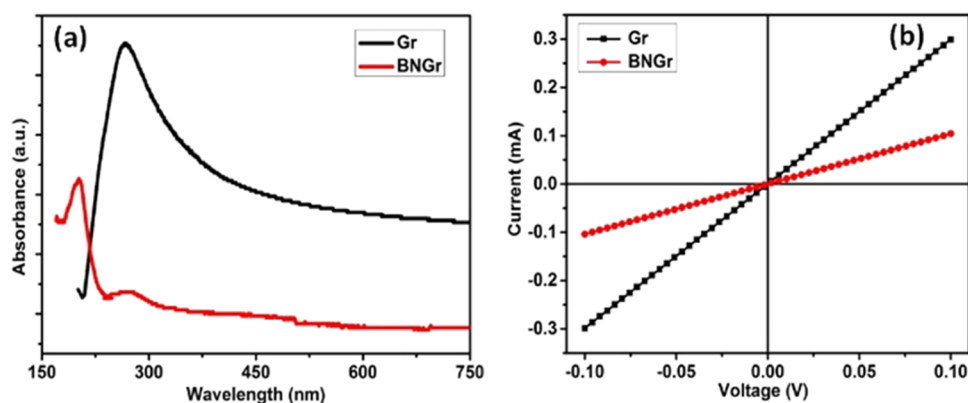


Figure 3. (a) UV–vis spectra of Gr and BNGr nanosheets on the quartz substrate. (b) *I*–*V* measurements of Gr and BNGr nanosheets on the Si/SiO₂ substrate.

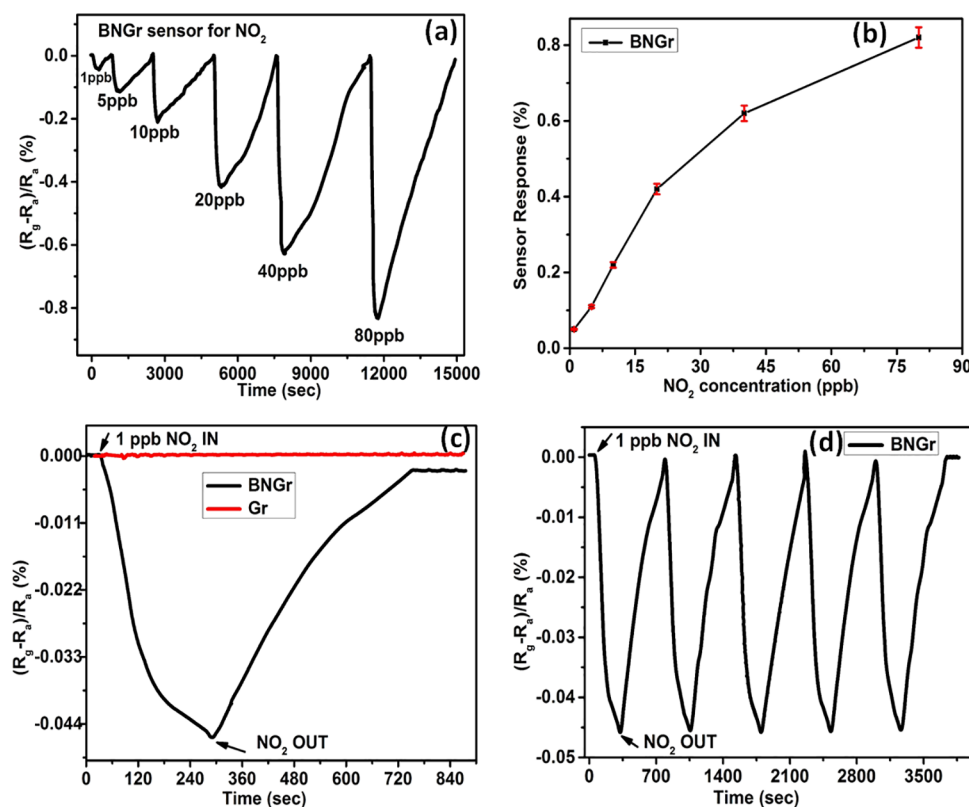


Figure 4. (a) Response versus time plots for 1–80 ppb NO₂ for the BNGr sensor. (b) Response versus ppb concentration of NO₂ for the BNGr sensor. (c) Comparison of sensor responses of Gr and BNGr sensors for 1 ppb NO₂. (d) Response curve of the BNGr sensor for five consecutive cycles of 1 ppb NO₂.

Table 4. Calculated Adsorption Energy (E_{ads} , eV), Equilibrium Graphene–Molecule Distance (d), and Bader Charge (\bar{e}) for the Adsorption of NO₂ Gas Molecules over Gr and BNGr Nanosheets

s. no.	system	adsorption energy for NO ₂ gas molecules (E_{ads} , eV)		equilibrium graphene–molecule distance [d] Å]		Bader charge gained by the adsorbed NO ₂ gas molecules from the atomic sheet
		present	other ^a	present	other ^a	present (Mulliken charge ⁶³)
1.	pure graphene (Gr) + NO ₂	−0.21	−0.48, ⁶³ +0.26 ⁶²	+3.12	+2.73, ⁶³ +2.98 ⁶²	+0.28 (−0.19)
2.	B–N-codoped graphene (BNGr) + NO ₂	−0.53	+1.3 ⁶³	+1.72		+0.67

^aThe + or − sign convention is just a way of representation, having same meaning in terms of explanation.

increases with the increase in NO₂ concentration from 1 to 80 ppb (Figure 4b). This could be very advantageous for the practical applications of the BNGr sensor in distinguishing the very low concentration of NO₂. The recovery of the sensors is also shown in consecutive cycles from 1 to 80 ppb. Initially, for the first cycle, the sensor was recovered very fast. As the time passed and with the increase in concentration, the sensor took a longer time to get recovered completely. This longer recovery time could be because of accumulation of some NO₂ gas molecules on the surface.

In Figure 4c, the single cycle of 1 ppb NO₂ for Gr and BNGr both has been shown to demonstrate the response and recovery cycle. It is clear from the figure that it has been very difficult for the Gr sensor to detect 1 ppb NO₂ gas, while there is a clearly visible change in the response value for the BNGr sensor. The response and recovery times for the BNGr sensor were also calculated and came out to be ~177 s to respond and ~392 s to recover completely for 1 ppb NO₂. Here, the response and recovery times have been defined as the time

required to achieve 90% of the response value and the time required to recover 90% of the cycle, respectively. To check the repeatability of the BNGr sensor, five consecutive cycles of sensing for 1 ppb NO₂ were recorded, as shown in Figure 4d. To further support the repeatability results, a graph for 50 consecutive cycles of sensing for 1 ppb NO₂ is also shown in Figure S6. The sensor shows an appreciable repeatability test.

Further, to discover underlying physics and validate our experimental results, we additionally carried out first-principles calculations for the adsorption energies of NO₂ molecules, graphene–molecule distance (d), and Bader charge (\bar{e}) gained by the adsorbed NO₂ gas molecules on graphene nanosheets. Table 4 summarizes the calculated values for both Gr and BNGr nanosheets. As it has been realized experimentally that the NO₂ gas molecule adsorption over graphene nanosheets may be enhanced by inducing defects such as doping of B or N and codoping of B–N at C sites into graphene.^{62,63} Therefore, to incorporate these B and N atoms into the study in accordance with our measurement, we followed the codoping

of B and N at about the center of the hexagonal graphene nanosheet. To predict energetically the most stable representative configuration of the BNGr system, we considered three possible configurations. Our microscopic analysis suggests that the codoping of B–N at regular sites, i.e., at the first nearest neighbor, is energetically more stable in comparison to the second and third nearest neighboring sites. The ground-state energy of the most stable configuration is lowered by 24.2 meV with respect to the least-stable configuration. Further, our calculation indicates that with the increase of the distance between B and N, the stability of the system deteriorates. Thus, the codoping of B–N into Gr forms strong bonding with each other and results in a B–N bond length of 1.45 Å. These predictions confirm our measurement of direct bond formation between B and N than C (as per XPS results). Furthermore, calculations of the adsorption of NO₂ gas molecules over the BNGr nanosheet have been performed and the structural parameters, system stability, and charge transfer properties have been extensively studied. Also, as per the theoretical study by Choudhuri I. et al.,⁶² in the case of B- and N-codoped graphene, the NO₂ gaseous molecules are adsorbed more strongly to B sites compared to N sites. With reference to this concept, we showed only the B sites for DFT calculations.

Our calculated lattice constant of Gr in the hexagonal lattice is equal to 2.46 Å. The calculated bond length between two consecutive C atoms into Gr is equal to 1.42 Å along with a bond angle of 120°, which are consistent with the available data.^{62,63} Next, the adsorption of NO₂ gas molecules over Gr and BNGr was performed and the stability of the system was predicted in terms of E_{ads} . From Table 4, it is clear that the adsorption of NO₂ gas molecules over Gr results in $E_{\text{ads}} = -0.21$ eV, which matches well with other calculated data.⁶⁴ The optimized structure of the adsorbed NO₂ gas molecules over Gr is shown in Figure 5a,c for top and side views. In the

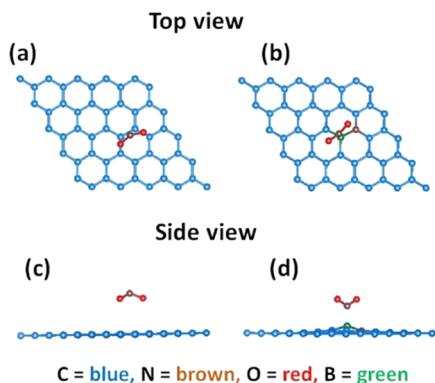


Figure 5. Optimized configurations (top and side views) for NO₂ gas molecule adsorption on (a, c) Gr and (b, d) BNGr. C, N, O, and B atoms are shown as blue, brown, red, and green solid spheres, respectively.

case when the adsorption of NO₂ gas molecules is followed over the BNGr nanosheet, the E_{ads} reduces sharply in comparison to that calculated for Gr. This shows that the stability of the system increases with the doping of B and N. In the case of codoping of B and N, we carefully checked the possibilities and chose the configuration that exhibits the lowest ground-state energy for NO₂ gas molecule adsorption, as shown in Figure 5b,d. Our microscopic study indicates that the codoping of B–N exhibits the lowest value of E_{ads} in

comparison to that calculated for the Gr nanosheet. It shows improvement in NO₂ gas sensing properties over BNGr than Gr. Our calculated E_{ads} follows the same trend as reported earlier.^{62,65} Moreover, our calculated optimized distance (d) between the NO₂ gas molecule and the closer atom of the Gr or BNGr nanosheet follows the same nature of decline, as presented in Table 4. For Gr, the largest numerical value is equal to 3.12 Å, which becomes smallest for the B–N-codoped system (1.70 Å), which shows improvement in NO₂ gas adsorption. To understand the transfer of electronic charges between the adsorbed NO₂ gas molecules and Gr and BNGr nanosheets, we performed Bader charge calculations.⁶⁴ Our calculation shows that the adsorbed NO₂ gas molecules gain electronic charges from the surrounded atoms of the Gr or BNGr nanosheet, which is smaller in the case of Gr, showing a very weak interaction of gas molecules. However, for the BNGr nanosheet, it is more than twice the calculated value for Gr and hence improves the gas sensing properties. Interestingly, these theoretical predictions support our experimental measurements in the context of enhancement of NO₂ gas sensing properties. The calculated results are summarized in Table 4. The complete baseline recovery of the BNGr sensor is observed even with higher adsorption energy for NO₂ in comparison to the Gr sensor. This suggests that NO₂ should be surface mobile.

From Figure 6, the calculated charge density difference for NO₂ gas molecules adsorbed on the Gr nanosheet surface

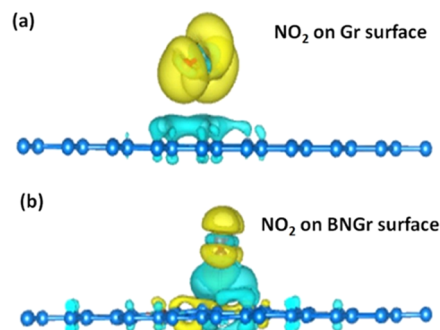


Figure 6. Charge density difference plots of the NO₂ gas molecule on (a) Gr surface and (b) BNGr surface.

clearly shows a very weak interaction due to no charge difference between them. However, a greater charge density appears between the adsorbed NO₂ gas molecule and the BNGr nanosheet, thus improving the interaction between them. These calculations are also consistent with our Bader charge calculations.

To have a proper comparison of the sensor response of BNGr with Gr, the higher concentrations (ppm) of NO₂ were also tested. For this, both the sensors were exposed to various concentrations of NO₂ from 5 to 80 ppm (Figure S7). For higher concentrations (ppm) also, the BNGr sensor shows an increased response with faster detection compared to the Gr sensor. The response values for both the sensors are shown in Table S1. Incorporation of B and N atoms in the graphene lattice increases the number of available active sites for NO₂ gas interaction in BNGr compared to Gr, and this may possibly be the reason for the increased response value of BNGr. Response and recovery cycles for both the sensors were also calculated and are given in Table S1. Here, the increase in recovery time for the BNGr sensor may possibly be because of

greater binding energy among the BNGr nanosheet and NO_2 gas. The gas sensing behavior for different concentrations of NO_2 shows that the sensors take a few minutes to recover to their actual resistances in normal conditions after each sensing cycle.

The relationship curves between the different concentrations of NO_2 from 5 to 80 ppm and their response values were also drawn for Gr and BNGr sensors, as shown in Figure S8a. They show that as the concentrations of NO_2 increase the response values increase. Hence, the BNGr sensor has better response values compared to those of the Gr sensor for higher concentrations also. To better evaluate the sensor results at ppm concentrations, the BN-codoped graphene sensor response was also compared with our previously reported N-doped graphene sensor,¹⁵ as shown in Figure S8b, to prove the necessity of codoping in graphene. To check the selectivity of the BNGr sensor, few commonly used gaseous species like chloroform, acetone, and ethanol were examined with the proposed sensor for 5 ppm NO_2 at room temperature. From Figure S9, it is clear that the BNGr sensor has a much higher response for NO_2 compared to other gaseous species.

4. SENSING MECHANISM

Fundamentally, the gas sensing abilities of any graphene material rely on the degree of interaction between the graphene layer and the gas molecule. Though a very precise mechanism of gas sensing is not known, the change in the carrier concentration and hence the change in resistance upon adsorption of gas molecules are accountable for the gas sensitivity property.¹³

In general, the direct charge transfer process between the adsorbed NO_2 molecules and graphene could be the most appropriate method to describe the sensing mechanism at room temperature. Figure 7 shows the schematic diagram of

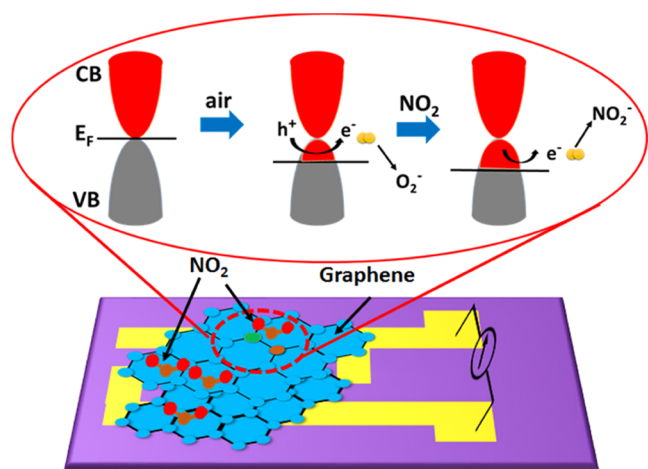


Figure 7. Schematic band diagram of the NO_2 gas sensing mechanism on the bilayer graphene nanosheet.

the sensing mechanism of the chemisorbed NO_2 gas molecule on the bilayer graphene-based gas sensor through the direct charge transfer process. It is assumed ideally that the Fermi level lies at the *K* point and the electronic band structure in bilayer graphene possesses a typical parabolic shape, which defines the finite charge carriers with effective mass. In ambient conditions, the air species (O_2^-) available on the graphene surface will receive electrons from its valance band and thus

induce holes and p-type conductivity. When NO_2 is exposed, the NO_2 molecules are adsorbed on the graphene surface and extract more electrons from its valance band (Figure 6).^{66,67} This increases the hole density, and as a result, the Fermi level shifts more toward the valance band.^{68,69} A bilayer graphene surface has a more available active area compared to a monolayer and hence more charge transfer is possible to NO_2 molecules. This larger charge transfer due to more adsorption leads to higher response values for NO_2 .

As per the literature, the interaction between any gas molecule and graphene particularly depends on the structure of graphene, i.e., doped or undoped, the required adsorption energy, and the configuration of how they are adsorbed.⁶³ The higher and lower values of responses for the Gr and BNGr sensors are decided by the power of this interaction. The triangular-shaped molecule of NO_2 gas can adsorb on graphene via three different possible configurations, which are nitro configuration (nitrogen end toward the graphene sheet), nitrile configuration (one oxygen end toward the graphene sheet), and cycloaddition configuration (both oxygen ends toward the graphene sheet). Each configuration has different adsorption energies when adsorbed on undoped and doped graphene nanosheets. Zhang et al.⁶³ calculated that the molecule of NO_2 adsorbs on undoped graphene via cycloaddition configuration with an adsorption energy of -0.48 eV. They further calculated that for N- and B-doped graphene, the interaction is through nitro configuration with the highest adsorption energies of -1.37 and -0.98 eV, respectively. These adsorption energy values conclude that both types of doping support the interaction of NO_2 gas molecules, and most probably, this could be the reason for the enhanced sensitivity of the BNGr sensor for NO_2 compared to the Gr sensor. The calculated adsorption energies in this study (Table 4) also support the reported studies and favor the enhanced sensitivity for NO_2 . Choudhuri I. et al.⁶² claimed in their study that when a gaseous molecule of NO_2 interacts with graphene codoped with both B and N, the adsorption is more at boron sites compared to nitrogen sites. They also calculated the adsorption energy for the NO_2 gas molecule and found it to be much higher (stronger) than those of their monodoped and pure structures. Being an oxidizing gas, NO_2 oxidizes B and a significant amount of charge carriers' (electrons) transfer takes place. Hence, these theoretical studies and calculations evidence that BN codoping can further enhance the interaction of NO_2 gas molecules than pure structures, and thus the BNGr sensor is ultrahigh sensitive for NO_2 .

5. CONCLUSIONS

In summary, the B- and N-codoped graphene nanosheets were synthesized successfully using the LPCVD method on a Cu foil substrate and were placed onto Si/SiO₂ for ultrahigh sensing of NO_2 at room temperature. In this work, the experimental work on the B- and N-codoped CVD graphene sensor for NO_2 detection at room temperature has been described. Several characterization techniques reveal that the heteroatoms B and N are doped in the graphene nanosheet and form bonds with C atoms. Because of the essential role of B and N, the proposed BNGr sensor demonstrates an ultrasensitive gas sensor for NO_2 gas. Importantly, the BNGr sensor exhibits a 0.05% response for 1 ppb NO_2 and a 3.29% response for 5 ppm NO_2 . These results reveal the significant role of heteroatom doping in graphene nanosheets. Furthermore, the BNGr sensor showcases the practical uses of the proposed

sensor to sense 1 ppb NO₂ with good repeatability and complete recovery at room temperature. The theoretical calculations performed in this study also support the enhancement in the sensor response of the graphene nanosheet after heteroatom doping. Thus, the proposed BNGr gas sensor may possibly be a superior alternative for designing next-generation ultrathin and low gravimetric gas sensors for compact device applications.

■ ASSOCIATED CONTENT

SI Supporting Information

The Supporting Information is available free of charge at <https://pubs.acs.org/doi/10.1021/acsmaterialsau.2c00003>.

LPCVD setup arrangement for BNGr nanosheet synthesis; FESEM and EDX images of the Gr nanosheet; deconvoluted C 1s spectra of Gr; O 1s core-level spectra of Gr and BNGr nanosheets; schematic of the gas sensing setup for sensing property measurement; response curve of the BNGr sensor for 50 consecutive cycles of 1 ppb NO₂; response curves for ppm concentrations of NO₂; table for response and recovery times; response of sensors as a function of the concentration of NO₂ gas in ppm of Gr and BNGr; comparison graph of the response of the BN-codoped graphene sensor with the N-doped graphene sensor as a function of the concentration of NO₂ gas in ppm; and selectivity of the BNGr sensor for 5 ppm NO₂ (PDF)

■ AUTHOR INFORMATION

Corresponding Authors

T. D. Senguttuvan – CSIR-National Physical Laboratory, New Delhi 110012, India; Academy of Scientific and Innovative Research (AcSIR), Ghaziabad 201002, India; Email: tdsen@nplindia.org

Bipin Kumar Gupta – CSIR-National Physical Laboratory, New Delhi 110012, India; Academy of Scientific and Innovative Research (AcSIR), Ghaziabad 201002, India; orcid.org/0000-0002-0176-0007; Email: bipinbhu@yahoo.com

Authors

Shubhda Srivastava – CSIR-National Physical Laboratory, New Delhi 110012, India; Academy of Scientific and Innovative Research (AcSIR), Ghaziabad 201002, India

Prabir Pal – Energy Materials and Devices Division, CSIR-Central Glass and Ceramic Research Institute, Kolkata 700032, India; Academy of Scientific and Innovative Research (AcSIR), Ghaziabad 201002, India; orcid.org/0000-0002-7356-2587

Durgesh Kumar Sharma – Applied Physics Department, Faculty of Engineering and Technology, M.J.P. Rohilkhand University, Bareilly 243006, India; Present Address: Theoretical Sciences Unit, Jawaharlal Nehru Centre for Advanced Scientific Research, Jakkur, Bangalore 560064, India

Sudhir Kumar – Applied Physics Department, Faculty of Engineering and Technology, M.J.P. Rohilkhand University, Bareilly 243006, India

Complete contact information is available at: <https://pubs.acs.org/doi/10.1021/acsmaterialsau.2c00003>

Notes

The authors declare no competing financial interest.

■ ACKNOWLEDGMENTS

The authors thank Director, CSIR-NPL, New Delhi. The authors also thank Vipin Kumar for his support in the design of the sensing setup. S.S. would like to thank Late Dr. Sushil Auluck for his guidance in theoretical measurements. X-ray photoelectron spectroscopy (XPS) measurements are performed at CSIR-Central Glass and Ceramic Research Institute (CGCRI), Kolkata. All of the theoretical calculations are performed on the High-Performance Computing (HPC) machine available at Physics Department, M.J.P. Rohilkhand University, funded under Science and Engineering Research Board (SERB), New Delhi vide project grant number SB/S2/CMP-033/2014. D.S.K. is thankful to SERB for financial support via grant number PDF/2020/002789.

■ REFERENCES

- (1) Kampa, M.; Castanas, E. Human health effects of air pollution. *Environ. Pollut.* **2008**, *151*, 362–367.
- (2) Ou, J. Z.; Ge, W.; Carey, B.; Daeneke, T.; Rotbart, A.; Shan, W.; Wang, Y.; Fu, Z.; Chrimes, A. F.; Wlodarski, W.; et al. Physisorption-based charge transfer in two-dimensional SnS₂ for selective and reversible NO₂ gas sensing. *ACS Nano* **2015**, *9*, 10313–10323.
- (3) Duy, L. T.; Kim, D. J.; Trung, T. Q.; Dang, V. Q.; Kim, B. Y.; Moon, H. K.; Lee, N. E. High performance three-dimensional chemical sensor platform using reduced graphene oxide formed on high aspect-ratio micro-pillars. *Adv. Funct. Mater.* **2015**, *25*, 883–890.
- (4) Yuan, W.; Huang, L.; Zhou, Q.; Shi, G. Ultrasensitive and selective nitrogen dioxide sensor based on self-assembled graphene/polymer composite nanofibers. *ACS Appl. Mater. Interfaces* **2014**, *6*, 17003–17008.
- (5) Wu, J.; Wu, Z.; Han, S.; Yang, B.-R.; Gui, X.; Tao, K.; Liu, C.; Miao, J.; Norford, L. K. Extremely deformable, transparent, and high-performance gas sensor based on ionic conductive hydrogel. *ACS Appl. Mater. Interfaces* **2019**, *11*, 2364–2373.
- (6) Wu, J.; Li, Z.; Xie, X.; Tao, K.; Liu, C.; Khor, K. A.; Miao, J.; Norford, L. K. 3D superhydrophobic reduced graphene oxide for activated NO₂ sensing with enhanced immunity to humidity. *J. Mater. Chem. A* **2018**, *6*, 478–488.
- (7) Li, Q.; Cen, Y.; Huang, J.; Li, X.; Zhang, H.; Geng, Y.; Yakobson, B. I.; Du, Y.; Tian, X. Zinc oxide–black phosphorus composites for ultrasensitive nitrogen dioxide sensing. *Nanoscale Horiz.* **2018**, *3*, 525–531.
- (8) Fowler, J. D.; Allen, M. J.; Tung, V. C.; Yang, Y.; Kaner, R. B.; Weiller, B. H. Practical chemical sensors from chemically derived graphene. *ACS Nano* **2009**, *3*, 301–306.
- (9) Hsu, L. C.; Ativanichayaphong, T.; Cao, H.; Sin, J.; Graff, M.; Stephanou, H. E.; Chiao, J. C. Evaluation of commercial metal-oxide based NO₂ sensors. *Sens. Rev.* **2007**, *27*, 121–131.
- (10) Chen, X.; Wang, T.; Han, Y.; Lv, W.; Li, B.; Su, C.; Zeng, M.; Yang, J.; Hu, N.; Su, Y.; et al. Wearable NO₂ sensing and wireless application based on ZnS nanoparticles/nitrogen-doped reduced graphene oxide. *Sens. Actuators, B* **2021**, *345*, No. 130423.
- (11) Wang, T.; Sun, Z.; Huang, D.; Yang, Z.; Ji, Q.; Hu, N.; Yin, G.; He, D.; Wei, H.; Zhang, Y. Studies on NH₃ gas sensing by zinc oxide nanowire-reduced graphene oxide nanocomposites. *Sens. Actuators, B* **2017**, *252*, 284–294.
- (12) Yavari, F.; Castillo, E.; Gullapalli, H.; Ajayan, P. M.; Koratkar, N. High sensitivity detection of NO₂ and NH₃ in air using chemical vapor deposition grown graphene. *Appl. Phys. Lett.* **2012**, *100*, No. 203120.
- (13) Schedin, F.; Geim, A. K.; Morozov, S. V.; Hill, E.; Blake, P.; Katsnelson, M.; Novoselov, K. S. Detection of individual gas molecules adsorbed on graphene. *Nat. Mater.* **2007**, *6*, 652–655.

- (14) Lv, R.; Li, Q.; Botello-Méndez, A. R.; Hayashi, T.; Wang, B.; Berkdemir, A.; Hao, Q.; Elías, A. L.; Cruz-Silva, R.; Gutiérrez, H. R.; et al. Nitrogen-doped graphene: beyond single substitution and enhanced molecular sensing. *Sci. Rep.* **2012**, *2*, No. 586.
- (15) Srivastava, S.; Kashyap, P. K.; Singh, V.; Senguttuvan, T.; Gupta, B. K. Nitrogen doped high quality CVD grown graphene as a fast responding NO₂ gas sensor. *New J. Chem.* **2018**, *42*, 9550–9556.
- (16) Zhang, H.; Fan, L.; Dong, H.; Zhang, P.; Nie, K.; Zhong, J.; Li, Y.; Guo, J.; Sun, X. Spectroscopic investigation of plasma-fluorinated monolayer graphene and application for gas sensing. *ACS Appl. Mater. Interfaces* **2016**, *8*, 8652–8661.
- (17) Park, M.-S.; Kim, K. H.; Kim, M.-J.; Lee, Y.-S. NH₃ gas sensing properties of a gas sensor based on fluorinated graphene oxide. *Colloids Surf., A* **2016**, *490*, 104–109.
- (18) Weng-Sieh, Z.; Cherrey, K.; Chopra, N. G.; Blase, X.; Miyamoto, Y.; Rubio, A.; Cohen, M. L.; Louie, S. G.; Zettl, A.; Gronsky, R. Synthesis of B x C y N z nanotubules. *Phys. Rev. B* **1995**, *51*, 11229.
- (19) Golberg, D.; Bando, Y.; Dorozhkin, P.; Dong, Z.-C. Synthesis, analysis, and electrical property measurements of compound nanotubes in the BCN ceramic system. *MRS Bull.* **2004**, *29*, 38–42.
- (20) Kaner, R.; Kouvetakis, J.; Warble, C.; Sattler, M.; Bartlett, N. Boron-carbon-nitrogen materials of graphite-like structure. *Mater. Res. Bull.* **1987**, *22*, 399–404.
- (21) Liu, A. Y.; Wentzcovitch, R. M.; Cohen, M. L. Atomic arrangement and electronic structure of BC₂N. *Phys. Rev. B* **1989**, *39*, 1760.
- (22) Miyamoto, Y.; Rubio, A.; Cohen, M. L.; Louie, S. G. Chiral tubules of hexagonal BC₂N. *Phys. Rev. B* **1994**, *50*, 4976.
- (23) Shinde, P. P.; Kumar, V. Direct band gap opening in graphene by BN doping: Ab initio calculations. *Phys. Rev. B* **2011**, *84*, No. 125401.
- (24) da Rocha Martins, J.; Chacham, H. Disorder and segregation in B–C–N graphene-type layers and nanotubes: tuning the band gap. *ACS Nano* **2011**, *5*, 385–393.
- (25) Tachikawa, H.; Iyama, T.; Azumi, K. Density functional theory study of boron-and nitrogen-atom-doped graphene chips. *Jpn. J. Appl. Phys.* **2011**, *50*, No. 01BJ03.
- (26) Xu, B.; Lu, Y.; Feng, Y.; Lin, J. Density functional theory study of BN-doped graphene superlattice: Role of geometrical shape and size. *J. Appl. Phys.* **2010**, *108*, No. 073711.
- (27) Ci, L.; Song, L.; Jin, C.; Jariwala, D.; Wu, D.; Li, Y.; Srivastava, A.; Wang, Z.; Storr, K.; Balicas, L.; et al. Atomic layers of hybridized boron nitride and graphene domains. *Nat. Mater.* **2010**, *9*, 430–435.
- (28) Li, L.; Yu, B.; You, T. Nitrogen and sulfur co-doped carbon dots for highly selective and sensitive detection of Hg (II) ions. *Biosens. Bioelectron.* **2015**, *74*, 263–269.
- (29) Gavvani, J. N.; Hasani, A.; Nouri, M.; Mahyari, M.; Salehi, A. Highly sensitive and flexible ammonia sensor based on S and N co-doped graphene quantum dots/polyaniline hybrid at room temperature. *Sens. Actuators, B* **2016**, *229*, 239–248.
- (30) Liu, R.; Zhao, J.; Huang, Z.; Zhang, L.; Zou, M.; Shi, B.; Zhao, S. Nitrogen and phosphorus co-doped graphene quantum dots as a nano-sensor for highly sensitive and selective imaging detection of nitrite in live cell. *Sens. Actuators, B* **2017**, *240*, 604–612.
- (31) Wang, Z.; Hu, H.; Zeng, H. The electronic properties of graphene nanoribbons with boron/nitrogen codoping. *Appl. Phys. Lett.* **2010**, *96*, No. 243110.
- (32) Jiang, H.; Zhao, T.; Shi, L.; Tan, P.; An, L. First-principles study of nitrogen-, boron-doped graphene and co-doped graphene as the potential catalysts in nonaqueous Li–O₂ batteries. *J. Phys. Chem. C* **2016**, *120*, 6612–6618.
- (33) Hosseini, A.; Asadi, Z.; Edjlali, L.; Bekhradnia, A.; Vessally, E. NO₂ sensing properties of a borazine doped nanographene: a DFT study. *Comput. Theor. Chem.* **2017**, *1106*, 36–42.
- (34) Niu, F.; Liu, J.-M.; Tao, L.-M.; Wang, W.; Song, W.-G. Nitrogen and silica co-doped graphene nanosheets for NO₂ gas sensing. *J. Mater. Chem. A* **2013**, *1*, 6130–6133.
- (35) Zheng, Y.; Jiao, Y.; Ge, L.; Jaroniec, M.; Qiao, S. Z. Two-step boron and nitrogen doping in graphene for enhanced synergistic catalysis. *Angew. Chem.* **2013**, *125*, 3192–3198.
- (36) Kattel, S.; Atanassov, P.; Kiefer, B. Density functional theory study of the oxygen reduction reaction mechanism in a BN co-doped graphene electrocatalyst. *J. Mater. Chem. A* **2014**, *2*, 10273–10279.
- (37) Esrafil, M. D.; Mousavian, P. Boosting graphene reactivity with co-doping of boron and nitrogen atoms: CO oxidation by O₂ molecule. *Appl. Surf. Sci.* **2018**, *455*, 808–814.
- (38) Kresse, G.; Furthmüller, J. Efficient iterative schemes for ab initio total-energy calculations using a plane-wave basis set. *Phys. Rev. B* **1996**, *54*, 11169.
- (39) Perdew, J. P.; Burke, K.; Ernzerhof, M. Generalized gradient approximation made simple. *Phys. Rev. Lett.* **1996**, *77*, 3865.
- (40) Grimme, S.; Antony, J.; Ehrlich, S.; Krieg, H. A consistent and accurate ab initio parametrization of density functional dispersion correction (DFT-D) for the 94 elements H–Pu. *J. Chem. Phys.* **2010**, *132*, No. 154104.
- (41) Ferrari, A. C.; Meyer, J.; Scardaci, V.; Casiraghi, C.; Lazzeri, M.; Mauri, F.; Piscanec, S.; Jiang, D.; Novoselov, K.; Roth, S.; et al. Raman spectrum of graphene and graphene layers. *Phys. Rev. Lett.* **2006**, *97*, No. 187401.
- (42) Casiraghi, C.; Pisana, S.; Novoselov, K.; Geim, A. K.; Ferrari, A. Raman fingerprint of charged impurities in graphene. *Appl. Phys. Lett.* **2007**, *91*, No. 233108.
- (43) Dong, X.; Shi, Y.; Zhao, Y.; Chen, D.; Ye, J.; Yao, Y.; Gao, F.; Ni, Z.; Yu, T.; Shen, Z.; et al. Symmetry breaking of graphene monolayers by molecular decoration. *Phys. Rev. Lett.* **2009**, *102*, No. 135501.
- (44) Yang, R.; Huang, Q.; Chen, X.; Zhang, G.; Gao, H.-J. Substrate doping effects on Raman spectrum of epitaxial graphene on SiC. *J. Appl. Phys.* **2010**, *107*, No. 034305.
- (45) Lee, J.; Novoselov, K. S.; Shin, H. S. Interaction between metal and graphene: dependence on the layer number of graphene. *ACS Nano* **2011**, *5*, 608–612.
- (46) Lei, W.; Portehault, D.; Dimova, R.; Antonietti, M. Boron carbon nitride nanostructures from salt melts: tunable water-soluble phosphors. *J. Am. Chem. Soc.* **2011**, *133*, 7121–7127.
- (47) Guimon, C.; Gonbeau, D.; P. ster-Guillouzo, G.; Dugne, O.; Guette, A.; Naslain, R.; Lahaye, M. XPS study of BN thin films deposited by CVD on SiC plane substrates. *Surf. Interface Anal.* **1990**, *16*, 440.
- (48) Kawaguchi, M. B/C/N materials based on the graphite network. *Adv. Mater.* **1997**, *9*, 615–625.
- (49) Ozaki, J.-i.; Kimura, N.; Anahara, T.; Oya, A. Preparation and oxygen reduction activity of BN-doped carbons. *Carbon* **2007**, *45*, 1847–1853.
- (50) Wei, D.; Liu, Y.; Wang, Y.; Zhang, H.; Huang, L.; Yu, G. Synthesis of N-doped graphene by chemical vapor deposition and its electrical properties. *Nano Lett.* **2009**, *9*, 1752–1758.
- (51) Bepete, G.; Voiry, D.; Chhowalla, M.; Chiguvare, Z.; Coville, N. J. Incorporation of small BN domains in graphene during CVD using methane, boric acid and nitrogen gas. *Nanoscale* **2013**, *5*, 6552–6557.
- (52) Park, K.; Lee, D.; Kim, K.; Moon, D. Observation of a hexagonal BN surface layer on the cubic BN film grown by dual ion beam sputter deposition. *Appl. Phys. Lett.* **1997**, *70*, 315–317.
- (53) Lin, T. W.; Su, C. Y.; Zhang, X. Q.; Zhang, W.; Lee, Y. H.; Chu, C. W.; Lin, H. Y.; Chang, M. T.; Chen, F. R.; Li, L. J. Converting graphene oxide monolayers into boron carbonitride nanosheets by substitutional doping. *Small* **2012**, *8*, 1384–1391.
- (54) Ismach, A.; Chou, H.; Ferrer, D. A.; Wu, Y.; McDonnell, S.; Floresca, H. C.; Covacevich, A.; Pope, C.; Piner, R.; Kim, M. J.; et al. Toward the controlled synthesis of hexagonal boron nitride films. *ACS Nano* **2012**, *6*, 6378–6385.
- (55) Cermignani, W.; Paulson, T. E.; Onneby, C.; Pantano, C. G. Synthesis and characterization of boron-doped carbons. *Carbon* **1995**, *33*, 367–374.

- (56) Jacobsohn, L.; Schulze, R.; Da Costa, M. M.; Nastasi, M. X-ray photoelectron spectroscopy investigation of boron carbide films deposited by sputtering. *Surf. Sci.* **2004**, *572*, 418–424.
- (57) Moreau, E.; Ferrer, F.; Vignaud, D.; Godey, S.; Wallart, X. Graphene growth by molecular beam epitaxy using a solid carbon source. *Phys. Status Solidi A* **2010**, *207*, 300–303.
- (58) Shao, Y.; Zhang, S.; Engelhard, M. H.; Li, G.; Shao, G.; Wang, Y.; Liu, J.; Aksay, I. A.; Lin, Y. Nitrogen-doped graphene and its electrochemical applications. *J. Mater. Chem.* **2010**, *20*, 7491–7496.
- (59) Morant, C.; Prieto, P.; Barenó, J.; Sanz, J.; Elizalde, E. Hard BC_xN_y thin films grown by dual ion beam sputtering. *Thin Solid Films* **2006**, *515*, 207–211.
- (60) Liu, B.; Yang, C.-M.; Liu, Z.; Lai, C.-S. N-doped graphene with low intrinsic defect densities via a solid source doping technique. *Nanomaterials* **2017**, *7*, 302.
- (61) Hawaldar, R.; Merino, P.; Correia, M.; Bdikin, I.; Grácio, J.; Méndez, J.; Martín-Gago, J.; Singh, M. K. Large-area high-throughput synthesis of monolayer graphene sheet by Hot Filament Thermal Chemical Vapor Deposition. *Sci. Rep.* **2012**, *2*, No. 682.
- (62) Choudhuri, I.; Patra, N.; Mahata, A.; Ahuja, R.; Pathak, B. B-N@ Graphene: highly sensitive and selective gas sensor. *J. Phys. Chem. C* **2015**, *119*, 24827–24836.
- (63) Zhang, Y.-H.; Chen, Y.-B.; Zhou, K.-G.; Liu, C.-H.; Zeng, J.; Zhang, H.-L.; Peng, Y. Improving gas sensing properties of graphene by introducing dopants and defects: a first-principles study. *Nanotechnology* **2009**, *20*, No. 185504.
- (64) Bader, R. F. A quantum theory of molecular structure and its applications. *Chem. Rev.* **1991**, *91*, 893–928.
- (65) Heyrovska, R. Atomic Structures of Graphene, Benzene and Methane with Bond Lengths as Sums of the Single, Double and Resonance Bond Radii of Carbon. 2008, arXiv:0804.4086. arXiv.org e-Print archive. <https://arxiv.org/abs/0804.4086> (accessed April 25, 2008).
- (66) Leenaerts, O.; Partoens, B.; Peeters, F. Adsorption of H_2O , NH_3 , CO , NO_2 , and NO on graphene: A first-principles study. *Phys. Rev. B* **2008**, *77*, No. 125416.
- (67) Jeong, S. Y.; Jeong, S.; Lee, S. W.; Kim, S. T.; Kim, D.; Jeong, H. J.; Han, J. T.; Baeg, K.-J.; Yang, S.; Jeong, M. S.; et al. Enhanced response and sensitivity of self-corrugated graphene sensors with anisotropic charge distribution. *Sci. Rep.* **2015**, *5*, No. 11216.
- (68) Akbari, E.; Yusof, R.; Ahmadi, M. T.; Enzevae, A.; Kiani, M.; Karimi, H.; Rahmani, M. Bilayer graphene application on NO_2 sensor modelling. *J. Nanomater.* **2014**, *2014*, No. 5.
- (69) Van Quang, V.; Van Dung, N.; SyTrong, N.; DucHoa, N.; Van Duy, N.; Van Hieu, N. Outstanding gas-sensing performance of graphene/ SnO_2 nanowire Schottky junctions. *Appl. Phys. Lett.* **2014**, *105*, No. 013107.